URSI GASS 2021, Rome, Italy, 28 August - 4 September 2021

Microwave Breast Imaging: Preliminary Phantoms Realization and Phaseless Reconstructions

Sandra Costanzo* (1), (2), (3), Giuseppe Lopez (1)
(1) DIMES, University of Calabria, Rende, Italy, costanzo@dimes.unical.it *
(2) CNR - Institute for Electromagnetic Sensing of the Environment (IREA), Naples, Italy
(3) ICEmB, Inter-University National Research Center on Interactions between Electromagnetic Fields and Biosystems, Genova, Italy

Abstract

In this work, a methodology involving amplitude-only microwave imaging, is described. The main features of the phaseless strategy are illustrated; then, some reconstruction scenarios are proposed, by investigating numerical breast models where the dielectric properties of the fabricated phantoms are integrated. Furthermore, in order to select the most suitable electromagnetic properties of the matching medium, a parametric modeling of a one-dimensional multi-layered structure is shown.

1 Introduction

Inverse scattering techniques have attracted an increasing interest in a variety of Microwave Imaging (MWI) applications, such as non-destructive testing, remote sensing and biomedical imaging. As for the latter, Microwave tomography (MWT) for breast imaging represents a major topic in the field of bio-electromagnetic research. In order to cope with the lack of accuracy that may arise in the phase retrieval stage [1], several phaseless reconstruction methods have been proposed [2]–[4]. As a matter of fact, the adoption of a phaseless reconstruction method can give a significant reduction in terms of complexity and overall cost of the acquisition system. A phaseless inversion scheme based on the Contrast Source (CS) approach is proposed and applied to a series of breast models, where the embedded dielectric properties are replaced with those provided by a series of realized phantoms.

2 Forward Modelling and Phaseless Inverse Problem

In this work, the inverse scattering problem is formulated according to the CS scheme [5], [6]. This method exploits phaseless acquisitions of the total filed, defined as the superimposition of the incident field and the field scattered by the Object Under Test (OUT). Since the imaging domain is an inaccessible region from a measurement perspective, the incident field distribution over the imaging domain is numerically evaluated as the field generated by a TM radiating source. Prior to experimental validation, the forward scattering problem, i.e. the evaluation of the electric field data originated from the presence of the target, needs to be solved. The forward problem is computed by implementing a conjugate-gradient Fast Fourier Transform (CG-FFT) solver [7]–[9]. According to a multistatic system approach, $N_{RX}=N_{TX}-1$ measurement points are considered for each TX position, resulting into $N_{TX}\cdot N_{RX}$ phaseless data for the total field. The EM profile of the target is iteratively reconstructed by adopting an optimization scheme. Together with the unknown dielectric contrast $\chi(r)=[\varepsilon_r(r)-\varepsilon_b]/\varepsilon_b$, where $\varepsilon_r(r)$ and ε_b are the relative complex permittivity of the imaging domain and of the matching medium, respectively, the induced current in the imaging domain, defined as $w(r)=\chi(r)\cdot E^{tot}$, is used as auxiliary unknown within the inversion scheme. Further details about the imaging strategy can be found in some previous papers by the authors [10]–[13].

3 Phantom realization and dielectric characterization

Prior to clinical trials, the realization of phantoms mimicking the electromagnetic (EM) properties of the human tissues provide an easy to fabricate and low-cost testbeds for preliminary experimental validations. Specifically, a series of phantoms are fabricated by using simple ingredients, which include water, sunflower oil, soap, salt and gelatine. As a generic guideline, the water/oil ratio is selected to cope with the lower (higher) dielectric permittivity values associated to tissues with low (high) water content. A food gelatine is used as solidifying agent, while dishwashing soap and salt are used to get a uniform final mixture and control the conductivity values, respectively. The EM properties of the realized phantoms are measured with a dielectric coaxial probe technique. For the case of fat and fibrogland phantoms, the EM properties are compared with the median curves of the models described in [14]. As for the blood tissue, whose EM properties are assumed to be similar to the ones of a tumor inclusion within the breast, a Cole-Cole model is considered as reference, following that reported in [15].

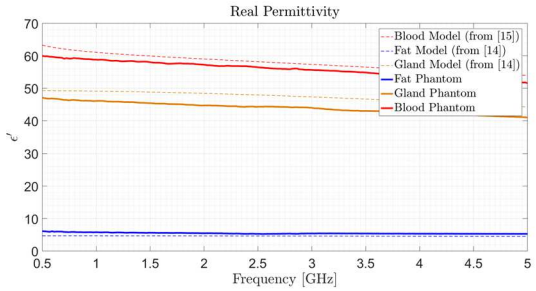

(a)

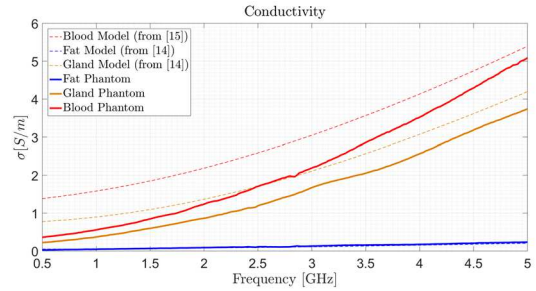

(b)

Fig. 1. EM properties of the fabricated phantoms (bold curves) compared to reference models provided in [14] and [15]; (a) relative permittivity and (b) conductivity.

The behaviors of the EM properties are shown in Fig. 1 and compared to the reference models, while the Root Mean Squared Error (RMSE) values are summarized in Table 1. In particular, the retrieved permittivity values well agree with the models for all the involved tissues. As for the conductivity values, the behaviors associated with the realized phantoms slightly differ from the references. However, by managing the salt percentage, a better agreement can be achieved.

Table 1. Root Mean Square Error (RMSE) of the phantoms' EM properties against the models.

Phantom Type	ε-RMSE	σ-RMSE [S/m]
Fat	0.87	0.02
Gland	3.36	0.51
Blood	2.00	0.83

4 On the matching medium selection: Transmission Line Model

Even though the internal breast structure is quite heterogeneous, as in other MWI imaging applications [16], [17], simplified propagation models can support the design of some features of the expected experimental system. For the case at hand, a 3-layered breast model is considered. Specifically, a parametric analysis is performed, in order to identify the more suitable permittivity range – and operating frequency – for the matching medium to be selected. The multi-layered structure consists of a 1.5 mm skin layer, a fat layer thickness of 35 mm, while the fibrogland region is assumed to be a semi-infinite layer. By exploiting a transmission line based model, the reflection coefficient at the matching medium-skin interface is evaluated, whose absolute value ($|\Gamma|$) is shown in Figure 2. From this preliminary analysis, it can be clearly noticed the high reflection in the case of the absence of a matching medium, while some low reflection regions can be identified. As a trade-off between energy coupling and penetration depth, a 2 GHz operating frequency and a relative permittivity for the matching medium in the range of 20 is selected. In the present work, we specifically assume ε_b=18.

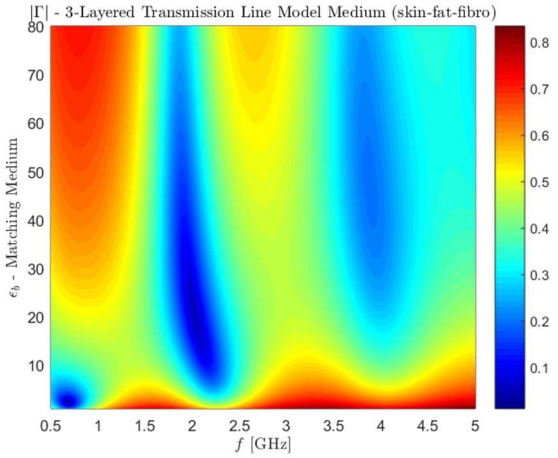

Fig. 2. $|\Gamma|$ map of the three-layered model, as function of frequency and relative permittivity of the matching medium ε_b.

5 Reconstruction Examples

The EM properties of the realized phantoms are exported within a series of realistic breast model provided in [18]. Those includes breast models with different fibrogland densities. For all models, a bloody region is included, to simulate a high permittivity tumor inclusion. The comparison between the ground truth profiles and the retrieved EM maps for the analyzed models is shown in Figure 2. For those reconstructions, N_{TX}=32 antenna locations have been assumed. The breast size is the only spatial prior assumed to be known. Despite the numerical difference between the retrieved and reference EM properties values and the limited resolution, the blood inclusion is located properly in the analyzed models, at least from a qualitative perspective.

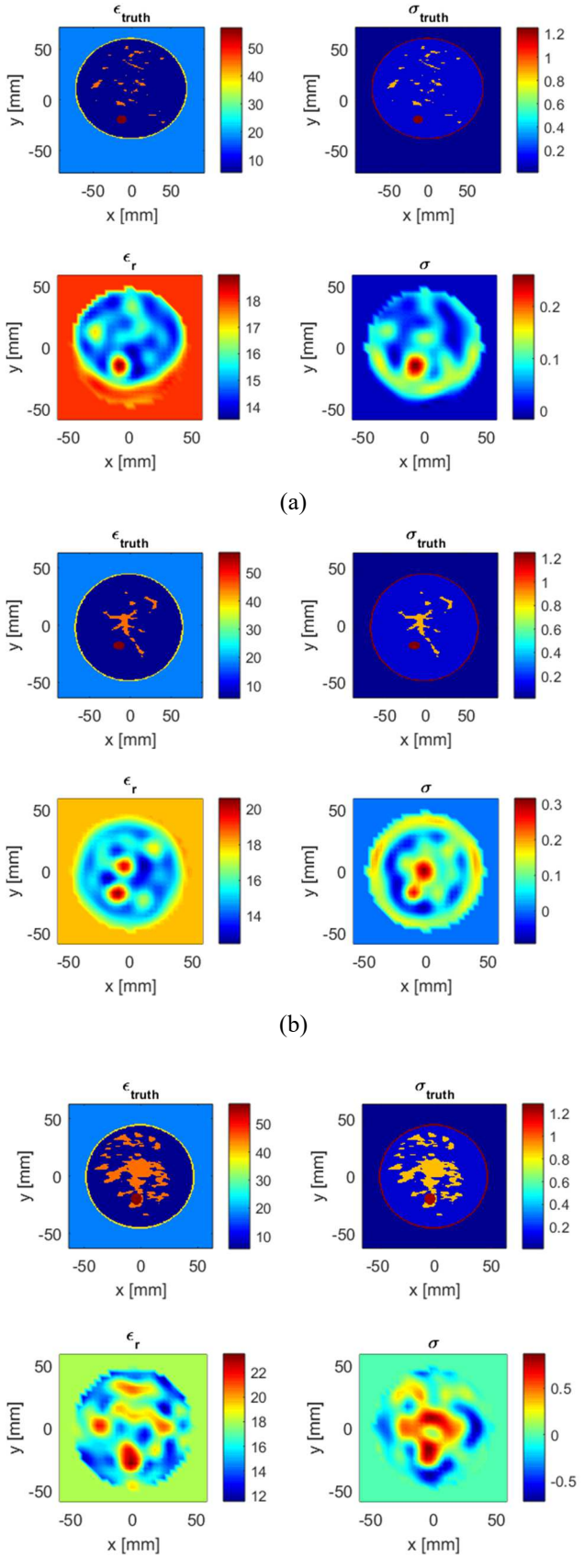

Fig. 3. Ground truth and EM reconstruction maps for a series of breast models: (a)-(b) mostly fatty, (c) scattered fibroglandular.

6 Conclusions

A summary of the microwave imaging activity and tissue mimicking phantom realization for breast imaging applications has been shown in this work. Specifically, the implemented imaging strategy exploits phaseless measurements of the total field data, generating two-dimensional EM properties distributions of a series of breast models. Prior to the inversion, the backscattered data is obtained from numerical breast models, where the dielectric properties of such models have been replaced by the ones obtained from a dielectric characterization of a series of mimicking tissue phantoms. The obtained results show the promising reconstruction capabilities of the proposed phaseless method, by opening to the experimental validation of an imaging setup which involves dielectric breast phantoms.

7 Acknowledgements

This work is co-financed by the European Social Fund (FSE) through the international mobility program of PhD students and Research grants/Researchers of type A - POR Calabria 2014-2020 - Actions 10.5.6 and 10.5.12.

8 References

1. A. Litman and K. Belkebir, “Two-dimensional inverse profiling problem using phaseless data,” *Journal of the Optical Society of America A*, **23**, 11, November 2006, p. 2737, doi: 10.1364/josaa.23.002737.
2. L. Pan, Y. Zhong, X. Chen, and S. P. Yeo, “Subspace-based optimization method for inverse scattering problems utilizing phaseless data,” *IEEE Transactions on Geoscience and Remote Sensing*, **49**, 3, March 2011, pp. 981–987, doi: 10.1109/TGRS.2010.2070512.
3. C. Narendra and P. Mojabi, “Phaseless Gauss-Newton Inversion for Microwave Imaging,” *IEEE Transactions on Antennas and Propagation*, **69**, 1, January 2021, pp. 443–456, doi: 10.1109/TAP.2020.3026427.
4. M. T. Bevacqua, G. G. Bellizzi, L. Crocco, and T. Isernia, “A method for quantitative imaging of electrical properties of human tissues from only amplitude electromagnetic data,” *Inverse Problems*, **35**, 2, February 2019, p. 025006, doi: 10.1088/1361-6420/aaf5b8.
5. P. M. Van Den Berg and R. E. Kleinman, “A contrast source inversion method,” *Inverse Problems*, **13**, 6, December 1997, pp. 1607–1620, doi: 10.1088/0266-5611/13/6/013.
6. P. M. Van Den Berg, A. L. van Broekhoven, and A. Abubakar, “Extended contrast source inversion,” *Inverse Problems*, **15**, 5, October 1999, pp. 1325–1344, doi: 10.1088/0266-5611/15/5/315.
7. T. J. Cui, W. C. Chew, X. X. Yin, and W. Hong, “Study of resolution and super resolution in

electromagnetic imaging for half-space problems," *IEEE Transactions on Antennas and Propagation*, **52**, 6, June 2004, pp. 1398–1411, doi: 10.1109/TAP.2004.829847.
8. X. Chen, *Computational methods for electromagnetic inverse scattering*. Wiley-IEEE Press.
9. Y. Qin, T. Rodet, M. Lambert, and D. Lesselier, "Microwave Breast Imaging With Prior Ultrasound Information," *IEEE Open Journal of Antennas and Propagation*, **1**, August 2020, pp. 472–482, doi: 10.1109/ojap.2020.3019953.
10. S. Costanzo and G. Lopez, "Phaseless Microwave Breast Imaging: Preliminary Study and Coupling Medium Effects," in *IMBioc 2020 - 2020 IEEE/MTT-S International Microwave Biomedical Conference*, 2020.
11. S. Costanzo and G. Lopez, "Phaseless Microwave Tomography Assessment for Breast Imaging: Preliminary Results," *International Journal of Antennas and Propagation*, **2020**, 2020, doi: 10.1155/2020/5780243.
12. S. Costanzo and G. Lopez, "Single-Step Approach to Phaseless Contrast-Source Inverse Scattering," Springer, Advances in Intelligent Systems and Computing, 2019, **932**, pp. 278–283, doi: 10.1007/978-3-030-16187-3_27.
13. S. Costanzo and G. Lopez, "Phaseless single-step microwave imaging technique for biomedical applications," *Radioengineering*, **28**, 3, 2019, doi: 10.13164/re.2019.0512.
14. M. Lazebnik *et al.*, "A large-scale study of the ultrawideband microwave dielectric properties of normal, benign and malignant breast tissues obtained from cancer surgeries," *Physics in Medicine and Biology*, **52**, 20, October 2007, pp. 6093–6115, doi: 10.1088/0031-9155/52/20/002.
15. S. Gabriel, R. W. Lau, and C. Gabriel, "The dielectric properties of biological tissues: III. Parametric models for the dielectric spectrum of tissues," *Physics in Medicine and Biology*, **41**, 11, November 1996, pp. 2271–2293, doi: 10.1088/0031-9155/41/11/003.
16. G. G. Bellizzi, K. Sumser, and M. T. Bevacqua, "On The Optimal Matching Medium and The Working Frequency in Deep Pelvic Hyperthermia," *IEEE Journal of Electromagnetics, RF and Microwaves in Medicine and Biology*, 2020, doi: 10.1109/JERM.2020.3047980.
17. C. Dachena, A. Fedeli, A. Fanti, M. B. Lodi, M. Pastorino, and A. Randazzo, "Microwave Imaging for the Diagnosis of Cervical Diseases: A Feasibility Analysis," *IEEE Journal of Electromagnetics, RF and Microwaves in Medicine and Biology*, 2020, doi: 10.1109/JERM.2020.3042711.
18. M. J. Burfeindt *et al.*, "MRI-derived 3-D-printed breast phantom for microwave breast imaging validation," *IEEE Antennas and Wireless Propagation Letters*, **11**, 2012, pp. 1610–1613, doi: 10.1109/LAWP.2012.2236293.